Insertion of lithium ion in anatase TiO_2 nanotube arrays of different morphology

Milan Bratić[a], Dragana Jugović[b], Miodrag Mitrić[c], Nikola Cvjetićanin[d*]

[a]*Vinča Institute of Nuclear Sciences, Laboratory for Atomic Physics, 11001 Belgrade, Serbia*

[b]*Institute of Technical Sciences of SASA, Knez Mihailova 35/IV, Belgrade, Serbia*

[c]*Vinča Institute of Nuclear Sciences, Laboratory for Theoretical and Condensed Matter Physics, 11001 Belgrade, Serbia*

[d]*Faculty of Physical Chemistry, University of Belgrade, Studentski trg 12-16, Belgrade, Serbia*

Abstract

Anatase TiO_2 nanotube arrays of different morphology were prepared by a two-step process: anodic oxidation at voltages 20-60V and subsequent annealing at 400^{o}C. By amplifying anodization voltage the inner diameter of nanotubes increased. At 60V nanotubes changed the shape from cylindrical tube to truncated cone with elliptical opening. Electrochemical insertion of Li-ion in nanotubes was studied by cyclic voltammetry and galvanostatic charge-discharge experiments. The cyclovoltammetric response was fast for all nanotube arrays. The galvanostatic areal charge/discharge capacity of nanotube arrays increased with increasing anodizaton voltage. Although the mass of nanotubes prepared at 45 V was larger, the gravimetrical capacity was much higher for nanotubes prepared at 60 V because of the larger surface area exposed to the electrolyte. Gravimetrical capacity values exceed theoretical bulk capacity of anatase due to the surface storage of Li-ion. Diffusion coefficient of Li-ion was calculated to be between $5.9 \cdot 10^{-16}$ and $5.9 \cdot 10^{-15}$ $cm^2 \cdot s^{-1}$.

Keywords: Nanostructured materials, Electrode materials, Electrochemical reactions, Diffusion, SEM, X-ray diffraction

*Corresponding author: Nikola Cvjetićanin, **nikola.cvj@ffh.bg.ac.rs**

1. Introduction

The possibility to grow TiO_2 nanotubes (NTs) by anodic oxidation has attracted much attention in the past two decades. The reason for this is the wide range of applications which are mostly based on semiconductive but also on potential biomedical properties of TiO_2. These applications generally include photocatalysis, electrochromic devices, solar cells, hydrogen storage, sensing applications, biomedical coatings, drug delivery and payload release systems [1,2]. Starting from Zwilling *et al*. in 1999 [3,4], who used water solutions of HF, different electrolytes containing fluoride anions were used for obtaining TiO_2 nanotube arrays (NTAs). It is worth mentioning that in 1979 Kelly may have already obtained TiO_2 NTs from F^-/H_2SO_4 solutions, but did not perform SEM with sufficient magnification for the evidence [5]. The breakthrough in the improvement of morphology of NTs was made by Macák et al. [6-9]. First, they demonstrated that by using neutral electrolytes containing NaF or NH_4F instead of HF the longer NTs were obtained [6-8]. Secondly, they showed that by using non-aqueous electrolytes smooth NTs without sidewalls inhomogeneity and the improved ordering could be obtained [9]. TiO_2 NTAs may be obtained by anodization in non-aqueous electrolytes containing 0.1-1 wt % of fluoride ions at the constant voltage between 5-150V [1] or even up to 350 V [10].

Intercalation of lithium ion into TiO_2 NTAs is interesting from two points of view: The first is the improvement of photoelectrochemical performance of NTs as the consequence of change of electronic structure upon Li^+ insertion [11]. The second is the potential application of NTAs as anode for lithium ion batteries (LIBs). In the last few years the investigations for LIBs applications involve amorphous titania NTAs [12, 13], anatase NTs [13,14], surface coated and modified NTs [15-17] and doped TiO_2 NTs [18].

In this paper the electrochemical insertion/extraction of lithium ion in anatase TiO_2 NTAs of different morphology was investigated by cyclic voltammetry and galvanostatic charge/discharge experiments. NTAs were prepared by anodization of Ti-foil in the solution of NH_4F in glycerol at voltages 20-60 V. The electrochemical lithiation/delithiation was investigated by exposing Ti/TiO_2-NTAs electrodes of the same geometrical surface area to the 1M solution of $LiClO_4$ in propylene carbonate (PC).

2. Experimental

2.1. Material preparation

TiO_2 NTAs were prepared by anodic oxidation of 0.25 mm thick and 0.5 cm wide Ti foil (Alfa Aesar, $\omega \geq 0.995$). The anodization was carried out in 0.7 % solution of NH_4F in glycerol by using graphite as a cathode, under constant voltage of 20, 30, 45 and 60 V during 6 hours. Ti-electrodes covered with TiO_2 NTAs, well rinsed with distilled water and dried, were annealed 3 hours in an air at 400 ^oC to convert TiO_2 from amorphous to crystal anatase form. These electrodes are designated, in further text, as 20V-TiO_2, 30V-TiO_2, 45V-TiO_2 and 60V-TiO_2 NTAs or NTs.

By anodic oxidation at 100-200 V, performed for 6 hours in 0.15% solution of NH_4F in glycerol [10], it was later found by SEM that film was obtained instead of NTs. TiO_2 film electrodes were not subjected to further investigation.

2.2. Electrode material characterization

The crystal structure of anodically grown TiO_2 was examined by X-ray diffraction (XRD). XRD data were collected by Philips PW diffractometer 1050 with Cu-Kα1,2 radiation in 2θ range 20-80^o with step size 0.05^o and counting time 2 s per step.

The morphology of obtained TiO_2 NTs was analyzed by JEOL JSM 6460LV scanning electron microscope.

Cyclic voltammetry (CV) was carried by Gamry PCI4/300 Potentiostat/Galvanostat in a bottle-like three-electrode cell. Ti-foil with anodically grown TiO_2 NTAs was used as working electrode and lithium metal foil was used both as reference and counter electrode. 1M solution of $LiClO_4$ in PC was used as electrolyte. $LiClO_4$ was dried overnight under reduced pressure at 130-150^{o}C and after that mixed with anhydrous PC. Both the electrolyte preparation and assembling of three-electrode cells was performed in argon filled glove-box. Geometrical surface area of working electrode in contact with electrolyte was 1 cm^2. The same cell in two electrode arrangement was used, after CV experiments, for galvanostatic charging/discharging experiments which were performed by Arbin BT 2042 battery testing device.

3. Results and discussion

3.1. Morphology and structure

The SEM micrographs in Fig. 1 show NTAs obtained by anodic oxidation of Ti-foil performed at 20-60 V. The inner diameter of NTs is around 60 nm at 20V, 80 nm at 30V and 110-140 nm at 45 V, Figs. 1A, 1B, 1C. For these voltages the inner diameter *d* of NTs follows a relationship $d\ (nm) = k \cdot U\ (V)$ [19], where constant *k* is ~3 for electrolyte used here. The thickness of NT walls does not depend significantly of anodization voltage and is around 35-40 nm. At 60 V the morphology of NTs is significantly changed in the sense that several NTs are merged into one whose inner diameter tapers as it goes to the top, Fig 1D. The openings of such NTs are mostly elliptical and range between 200 and 400 nm and NTs take the form resembling truncated cone. Such change in morphology most likely comes from the fact that 60 V is limiting voltage for obtaining NTs at concentration 0.7% of NH_4F in glycerol. According to Alivov et al. [10] concentration of NH_4F must be decreased for obtaining TiO_2 NTAs at higher voltages.

XRD patterns of pristine Ti-foil and TiO_2 NTs obtained by anodic oxidation of Ti-foil at 20, 30, 45 and 60V, and submitted to thermal treatment in air at 400^{o}C, are shown in Fig. 2**.** The pristine Ti-foil consists of Ti-metal (PDF-2 89-2959) with a small amount of TiO (PDF-2 86-2352) on the surface. TiO phase disappears after anodization. The reflections of anatase phase are clearly visible and agree with the literature data (PDF-2 86-1156). The relative intensity of the strongest reflection of anatase phase at 25^o (2θ) increases with increasing voltage up to 45V and then decreases for the highest voltage of 60V, Table 1. The thicker NT layer, after annealing at 400^{o}C, would give higher intensity of diffraction maximums of anatase phase relatively to Ti-foil. The linear increase and then saturation and decrease in the thickness of NT layer, was observed before for glycerol based electrolytes with the increase of anodization voltage. Such saturation was ascribed to the thinning of NT walls [19]. Additional reflections of small

intensity can be observed for foil anodized at 60V which agree with the reflections that come from the theoretically calculated Ti-metal fcc lattice (PDF-2 88-2321). The X-ray Line Profile Fitting with Program (XFIT) with a Fundamental Parameters convolution approach to generating line profiles was used for the calculation of the mean crystallite size [20]. The mean crystallite size of anatase NTAs does not change much, but has a tendency to decrease with an increase of the applied anodization voltage, Table 1.

3.2.Electrochemistry

3.2.1. Cyclic voltammetry

The CV curves of anatase TiO_2 NTAs, obtained at anodization voltages 20-60 V, are recorded at scan rates 1 to 20 mV s^{-1} in the potential range from 3 to 1 V vs. Li/Li^+ at room temperature, Fig. 3. At all scan rates, for all NTAs, Ti^{4+}/Ti^{3+} redox peaks appear designating very fast intercalation/deintercalation kinetics, usually observed in water based electrolytes, but not typical for organic ones [21]. Cathodic and anodic peak current increases at all scan rates when anodization voltage is amplified up to 45V, but then decreases at 60 V. However, even at the lowest scan rate of 1 $mV \cdot s^{-1}$ redox peak-to-peak separation, which amounts 0.457-0.484 V is significantly larger than the Nernstian. Nevertheless, similar peak-to-peak separation in CV experiments was also observed earlier for TiO_2 NTs in different electrolytes [13, 14, 22]. The absence of better reversibility may be attributed to slow electron transport through semiconducting TiO_2 NTs. Despite that, the fast CV response most likely comes from short diffusion length of Li^+ ion into 35-40 nm thick nanotube walls. In addition to larger redox peaks, smaller peaks can be also observed at all scan rates. While in reduction this smaller peak is clearly visible, in oxidation this peak is very wide and can be easily overlooked. These smaller

peaks may come from some additional filling of oxygen octahedra with lithium ion, above composition $Li_{0.5}TiO_2$, which is energetically less favorable [23].

According to equations both for reversible and irreversible electrochemical reactions, the slope of logi_p vs. logυ should be 0.5 [24]. For NTAs obtained at all voltages the slope for cathodic and anodic peak currents was between 0.486 and 0.502 and between 0.502 and 0.532, respectively, (Supplementary data). According to these data the process of both insertion and extraction of lithium ion can be considered as diffusion controlled. However, it should be remembered that capacitive contribution to voltammetric peaks is not small for anatase, but is the least pronounced at current maxima [25]. On the basis of equation for irreversible electrochemical reaction [24]:

$$i_p = 0.4958nFACD^{1/2}\left(\frac{\alpha n_a F}{RT}\right)^{1/2}\upsilon^{1/2} \qquad (1)$$

the cathodic and anodic peak current as a function of square root of scan rate was plotted for all anodization voltages, Fig 4. All the data can be fitted with the straight line whose intercept is close to zero, which confirms the validity of equation (1). The slope of the line increases with the increase of anodization voltage up to 45 V and then decreases at 60 V. The slope depends only from two variables: surface area - *A* and diffusion coefficient – *D*. Lindström *et al.* [26] demonstrated that peak split and peak height do not depend on the concentration of Li^+ ions in the electrolyte. The concentration *C* in equation (1) can be taken as the maximum obtainable concentration of Ti^{3+} in the lattice and amounts 0.0236 mol·cm^{-3} for composition x = 0.5

($Li_{0.5}TiO_2$). The other quantities on the right side of equation (1) are universal constants or can be taken to have constant value.

3.2.2. Galvanostatic experiments

The galvanostatic cycling was performed by using the same current density 50 $\mu A \cdot cm^{-2}$ (geometric surface area) for all Ti/TiO_2 NTAs electrodes. The galvanostatic charge/discharge (lithium extraction/lithium insertion) areal capacity of NTAs, shown for 50 cycles in Fig. 5, increases by increasing anodization voltage. The discharge capacity retention after 50 cycles is excellent for NTs obtained at 20, 30 and 45 V, while for NTs obtained at 60V capacity fading during discharge can be observed. The coulombic efficiency in the last 20 cycles is around 100% for 20V-TiO_2 NTAs, but slightly decreases when anodization voltage is further amplified to 30 V and further to 45 V, Fig. 6. In the case for 60V-TiO_2 NTAs much lower coulombic efficiency can be observed, however it shows increasing trend and it is possible that larger number of charge-discharge cycles is required to stabilize this electrode. On the other hand, if decomposition of electrolyte decreases the coulombic efficiency it will be most pronounced for NTAs with highest surface area. The increase in cathodic current with the approach of a voltage to 1.0 volts vs Li/Li^+ in CV experiments, Fig. 3, and the fact that this current, comparing to cathodic peak current, is highest for 60V-TiO_2 NTAs supports the existence of electrolyte reduction in the vicinity of lower cut-off voltage.

The voltage profiles for the 50th cycle for all anodization voltages are compared in Fig. 7a. The region where the voltage is constant reflects phase transition between two phases: Li-poor $Li_{0.026}TiO_2$ and Li-rich $Li_{0.52}TiO_2$ [23, 27]. The region with inclined voltage profile, down

to 1.0 V, designates the existence of surface storage mechanism [27, 28]. In this case free energy during lithiation is not constant but decreases incrementally as a function of lithium ion concentration because surface of NTs acts as a solid solution host to lithium ion insertion [29]. The small inflection region around 1.45 V, on the inclined part of discharge voltage profiles, may be the attempt of forming of a second voltage plateau – phase transition between Li-rich $Li_{0.52}TiO_2$ and Li_1TiO_2 phase. Wagemaker's group has shown that both phase transitions are a nonequilibrium transformation, and they suggested that second phase transition is a characteristic of very small anatase particles, smaller than 15nm [30]. However, the experiments of Jiang *et al.* [28] probably confirm the assumption outlined here, because in them the same small inflection region can be observed for particles of crystallite size 30 nm and also the enlargement of that region for particles of crystallite size 6 nm. The small capacity values that correspond to initial voltage drop, from 3 V down to flat region, also grow with increasing anodic oxidation voltage and most likely may be attributed to electrochemical double layer capacitance which is as well proportional to specific surface area [28]. For the calculation of capacities of inclined and flat part during discharge the points of minimum curve radius of concave and convex part of each voltage profile were taken, as middle-points during the change from one storage mechanism to another, Fig.7a. The ratio of capacities of inclined and flat part during discharge (lithium insertion) is similar for NTs obtained at 20, 30 and 45 V and amounts 0.81, 0.82 and 0.84, respectively. The increase of inner diameter enables better penetration of electrolyte inside NTs and probably between NTs because of the enlarged space among them. This increases the number of sites for intercalation of Li^+ ion into single NT. Unfortunately this also decreases the number of NTs per unit surface area which are in contact with electrolyte.

Therefore, the increase of NTs length, by amplifying anodization voltage from 20 to 45 V, may be the main reason for the increase of areal capacity. The increase of NTs length is in content with the gain in amount of anatase phase observed by XRD, Table 1, when anodic oxidation voltage is enhanced in the range 20-45 V. The ratio of surface to bulk capacity is much higher for 60V-TiO_2 NTs and is equal to 1.08. The increase of ratio between surface and bulk capacity was found earlier in particle size reduction of nanocrystalline anatase [27, 28]. The largest value of capacity of inclined part demonstrates, and confirms an earlier assumption, that 60V-TiO_2 NTAs have the largest surface area exposed to electrolyte. The significantly increased inner diameter, conical shape and rippled walls of 60V-TiO_2 NTs enable enlargement of contact area with electrolyte both from inside and outside of NTs, Fig 1d.

The capacity of sloped region in charge, from 1.0 V up to ~1.94 V, also increases with increasing anodization voltage. At the beginning of plateau, upon charge, the potential is overdriven for 20V-, 30V- and 45V-TiO_2 NTs, Fig. 7b, which is assigned to a nucleation barrier for the phase transition from Li-rich to Li-poor phase [31]. The nucleation barrier decreases with increasing anodization voltage and completely disappears for highest voltage - 60V. Since crystallite size also gradually decreases with the increase of anodization voltage, Table 1, this indicates step by step transition from larger two phase domains to smaller domains with either first or second phase [30, 31].

Determination of gravimetric insertion/deinsertion capacity demands the mass of NTs. By scraping NTs from Ti-foil their mass was determined with sufficient accuracy only for anodic oxidation performed at 45 V and 60 V. The obtained mass of 60V-TiO_2 NTs is lower than mass of 45V-TiO_2 NTs, which is in accordance with the relative amount of anatase phase from XRD

data, Table 1. The voltage profiles for the 50th cycle show much higher both bulk and surface storage specific capacity of 60V-TiO_2 NTs, Fig. 7c. The specific charge/discharge capacity of 45V-TiO_2 NTAs is very stable, Fig. 8 and amounts 190 $mAh \cdot g^{-1}$ at current rate 0.93 C. Slight periodical variation in capacity is due to lower temperature in the laboratory overnight. The specific charge/discharge capacity of 60V-TiO2 NTAs is as high as 260/285 $mAh \cdot g^{-1}$ after 50 cycles at current rate 1.17 C. Such large capacity at this current rate must be attributed, in the first place, to the large contribution of surface storage of lithium ion which does not depend on bulk diffusion time [28]. The easily noticeable difference between charge and discharge capacity, as pointed above, is most likely due to electrolyte decomposition around 1.0V vs Li/Li^+. The decomposition of the electrolyte, as a separate topic, is not considered in this paper, but one proposed mechanism is a reduction of cyclic ester on the surface of TiO_2 with strongly adsorbed water [32]. The discharge capacity of 45V-TiO_2 NTs is higher than values obtained for amorphous TiO_2 NTAs, synthesized by anodization at 20 and 30 V and cycled at current rate of 1/3 C [12] and very similar to capacity of hydrothermally synthesized and carbon-coated anatase TiO_2 NTs at current rate 1 C [31]. Much higher discharge capacity of 60V-TiO_2 NTs at current rate close to 1C is very similar to that of very thin electrode prepared from anatase TiO_2 NTs obtained by combined hydrothermal reaction and annealing at 300^oC [33].

Galvanostatic experiments showed that anatase NTAs can exhibit characteristics that are usually only found in very small nanoparticles. The larger surface than bulk storage capacity of Li^+ ion and disappearance of nucleation barrier can occur with NTAs, although this might not be expected on the basis of morphology and crystallite size. Despite the fact that small nanoparticles usually have larger surface to bulk storage capacity, electrodes based on them [28, 34]

demonstrate lower discharge capacity retention comparing to robust Ti/TiO_2 NTs electrodes obtained here.

3.2.3. Determination of diffusion coefficient

The chemical diffusion coefficient of lithium ions was calculated for NTAs obtained at all anodization voltages. For electrode with 60V-TiO_2 NTs, which have the most accessible surface, by using specific surface area of 30 $m^2 \cdot g^{-1}$ [35], the surface area of NTs was calculated to be ~77 cm^2. By using the ratio of inclined parts of voltage profiles during discharge, Fig. 7a, the surface area of 45V-TiO_2 NTs was obtained to be 56.8 cm^2, which corresponds to specific surface area of 17.8 $m^2 \cdot g^{-1}$. The surface area of 20V-TiO_2 NTs and 30V-TiO_2 NTs were calculated in the same manner and shown in Table 2. From equation (1) and the slope of cathodic and anodic peak current as a function of square root of scan rate, Fig. 5, by taking, n = n_a =1, α = 0.5, R = 8.314 $J \cdot mol^{-1}K^{-1}$, F = 96500 $C \cdot mol^{-1}$, T = 295 K, C = 0.0236 $mol \cdot cm^{-3}$, and finally the calculated surface area, the diffusion coefficient was calculated both for insertion extraction of lithium ion, Table 2. The obtained values are similar for insertion and extraction, for each anodization voltage, and are in the range from $5.9 \cdot 10^{-16}$ $cm^2 \cdot s^{-1}$ to $5.9 \cdot 10^{-15}$ $cm^2 \cdot s^{-1}$. These values are one to two orders of magnitude higher than those obtained in a similar manner for 0.11 μm and 4.2 μm thick nanoporous TiO_2 anatase electrode [26], but very similar to values obtained for lithium ion diffusion into anatase TiO_2 grains sized between 20 and 135 nm [36]. The decrease of diffusion coefficients of lithium ion most likely is due to the increase of electrical resistivity of NTs with the increase of anodization voltage [10]. The lower diffusion coefficient may be responsible for the increase of the ratio of surface to bulk capacity.

Conclusions

The electrochemical insertion of lithium ion in anatase TiO_2 nanotube arrays of different morphology, obtained by anodization at 20-60 V and subsequent annealing at 400^{o}C, has been investigated. It was shown that insertion capacity of nanotube arrays may significantly overshoot theoretical bulk capacity of anatase phase, at current rate ~ 1 C, due to the surface storage of lithium which does not depend on slow bulk diffusion. Practically no capacity fade was observed during discharge for all nanotubes, except for those prepared at the highest anodic oxidation voltage. The increase of surface area of nanotubes in contact with electrolyte improves lithium insertion rate capabilities, but may give rise to electrolyte reduction-decomposition which decreases coulombic efficiency. The nucleation barrier disappears during lithium extraction from nanotube arrays obtained by anodic oxidation at 60 V. This may be explained by the absence of larger two phase domains and the existence of smaller domains with either first - Li-rich phase or second - Li-poor phase.

Considering that Ti/TiO_2-NTAs electrode combines concurrently current collector and anode material, it is very promising for development of durable ultra-thin lithium-ion batteries. Tailoring nanotube arrays morphology may significantly improve the performances of anodes for such batteries.

Acknowledgment

The Ministry of Science and Technological Development of Republic Serbia supported this work (Project No. III 45014, III 45015, III 45004).

References

[1] X. Chen and S. S. Mao, Titanium dioxide nanomaterials: synthesis, properties, modifications and applications, Chem. Rev 107 (2007) 2891-2959

[2] P. Roy, S. Berger, P. Schmuki, TiO_2 nanotubes: synthesis and applications, Angew. Chem. Int. Ed. 50 (2011) 2904–2939

[3] V. Zwilling, E. Darque-Ceretti, Boutry-Forveille, D. David, M. Y. Perrin, M. Aucouturier, Structure and physicochemistry of anodic oxide films on titanium and TA6V alloy. Surf. Interface Anal. 27 (1999) 629-637

[4] V. Zwilling, M. Aucouturier E. Darque-Ceretti, Anodic oxidation of titanium and TA6V alloy in chromic media. An electrochemical approach, Electrochim. Acta 45 (1999) 921-929

[5] J. J. Kelly, The influence of fluoride ions on the passive dissolution of titanium, Electrochim. Acta 24 (1979) 1273-1282

[6] J. M. Macák, K. Sirotna, P. Schmuki, Self-organized porous titanium oxide prepared in Na_2SO_4/NaF electrolytes, Electrochim. Acta 50 (2005) 3679-3684

[7] J. M. Macák, H. Tsuchiya, P. Schmuki, High-aspect-ratio TiO_2 nanotubes by anodization of titanium, Angew. Chem. Int. Ed. 44 (2005) 2100-2102

[8] L. V. Taveira, J. M. Macák, H. Tsuchiya, L. F. P. Dick, and P. Schmuki, Initiation and growth of self-organized TiO_2 nanotubes anodically formed in $NH_4F/(NH_4)_2SO_4$ electrolytes, J. electrochem. Soc. 152 (2005) B405-B410

[9] J. M. Macák, H. Tsuchiya, L. Taveira, S. Aldabergerova, P. Schmuki, Smooth anodic TiO_2 nanotubes, Angew. Chem. Int. Ed. 44 (2005) 7463-7465

[10] Y. Alivov, M. Pandikunta, S. Nikishin, Z.Y. Fan, The anodization voltage influence on the properties of TiO2 nanotubes grown by electrochemical oxidation, Nanotechnology 20 (2009) 225602

[11] B. H. Meekins, P.V. Kamat, Got TiO_2 nanotubes? Lithium ion intercalation can boost their photoelectrochemical performance, ASC Nano 3(11) (2009) 3437–3446

[12] Q. L. Wu, J. Li, R. Deshpande, N. Subramanian, S. E. Rankin, F. Yang, Y.-T. Cheng, Aligned TiO_2 nanotube arrays as durable lithium-ion battery negative electrodes, J. Phys. Chem. C 116 (2012) 18669–18677

[13] S.-G. Park, J.-J. Yang, J.W. Rho, H.-I. Kim, H. Habazaki, Electrochemical behavior of TiO_2 nanotube/Ti prepared by anodizing for micro-lithium ion batteries, J. Korean Electrochem. Soc. 17 (2014) 13–17

[14] R.G. Freitas, S.G. Justro, E.C. Pereira, The influence of self-ordered TiO_2 nanotubes microstructure towards Li^+ intercalation, J. Power Sources 243 (2013) 569-572

[15] J. Brumbarov, J. Kunze-Liebhäuser, Silicon on conductive self-organized TiO_2 nanotubes – A high capacity anode material for Li-ion batteries, J. Power Sources 258 (2014) 129-133

[16] D. Bresser, B. Oschmann, M. N. Tahir, F. Mueller, I. Lieberwirth, W. Tremet, R. Yentel, S. Passerini, Carbon-Coated Anatase TiO_2 Nanotubes for Li- and Na-Ion Anodes, J. Electrochem. Soc. 162 (2015) A3013-A3020

[17] G. F. Ortiz, M. Cabello, M.C. López, J.L. Tirado, M.J. McDonald, Y. Yang, Exploring a Li-ion Battery using surface modified titania nanotubes versus high voltage cathode nanowires, J. Power Sources 303 (2016) 194-202

[18] N.A. Kyerameteng, F. Vacandio, M.-T. Sougrati, H. Martiney, J.-C. Jumas, P. Knauth, T. Djenizian, Effect of Sn-doping on the electrochemical behaviour of TiO_2 nanotubes as potential negative electrode materials for 3D Li-ion micro batteries, J. Power Sources 224 (2013) 269-277

[19] J. M. Macák, H. Hildebrand, U. Marten-Jahns, P. Schmuki, Mechanistic aspects and growth of large diameter self-organized TiO_2 nanotubes, J. Electroanal. Chem. 621 (2008) 254-266

[20] R. W. Cheary, A. Coelho, A fundamental parameters approach to X-ray line-profile fitting, J. appl. Crystallogr. 25 (1992) 109-121

[21] M. Vujković, D. Jugović, M. Mitrić, I. Stojković, N. Cvjetićanin, S. Mentus, The $LiFe_{(1-x)}V_xPO_4$/C composite synthesized by gel-combustion method, with improved rate capability and cycle life in aerated aqueous solutions, Electrochim. Acta 109 (2013) 835–842

[22] D. Fang, K. Huang, S. Liu, Z. Li, Electrochemical properties of ordered TiO_2 nanotube loaded with Ag nano-particles for lithium anode material, J. Alloy. Compd. 464 (2008) L5–L9

[23] M. Wagemaker, G.J. Kearley, A.A. van Well, H. Mutka, F.M. Mulder, Multiple Li positions inside oxygen octahedra in lithiated TiO_2 anatase, J. Am. Chem. Soc. 125 (2003) 840–848

[24] A. J. Bard, L. R. Faulkner, Electrochemical methods: Fundamentals and applications, second ed., John Wiley & Sons, New York (2001), Chapter 6.

[25] B. Laskova, M. Zukalova, A. Zukal, M. Bousa, L. Kavan, Capacitive contribution to Li-storage in TiO_2 (B) and TiO_2 (anatase), J. Power Sources 246 (2014) 103-109

[26] H. Lindström, S. Södergren. A. Solbrand, H. Rensmo, J. Hjelm, A. Hagfeldt. S.E. Lindquist, Li^+ ion insertion in TiO_2 (anatase). 2. Voltammetry on nanoporous films, J. Phys. Chem. B 101 (1997) 7717-7722

[27] M. Wagemaker, F. M. Mulder, Properties and promises of nanosized insertion materials for Li-ion batteries, Acc. Chem. Res. 46 (2013) 1206–1215

[28] C. Jiang, M. Wei, Z. Qi, T. Kudo, I. Honma, H. Zhou, Particle size dependence of the lithium storage capability and high rate performance of nanocrystalline anatase electrode, J. Power Sources 166 (2007) 239-243

[29] A. G. Dylla, G. Henkelman, K. J. Stevenson, Lithium insertion in Nanostructural TiO_2 (B) Architectures, Acc. Chem. Res. 46 (2013) 1104–1112.

[30] K. Shen, H. Chen, F. Klaver, F. M. Mulder, M. Wagemaker, Impact of particle size on the non-equilibrium phase transition of lithium inserted anatase TiO_2, Chem. Mater. 26 (2014) 1608-1615

[31] D. Bresser, B. Oschmann, M. N. Tahir, F. Mueller, I. Lieberwirth, W. Tremel, R. Zentel, S. Passerini, Carbon-coated anatase TiO_2 nanotubes for Li- and Na-ion batteries, J. Electrochem. Soc. 162 (2015) A3013-A3020

[32] W. J. H. Borghols, D. Lützenkirchen-Hecht, U. Haake, W. Chan, U. Lafont, E. M. Kelder, E. R. H. van Eck, A. P. M. Kentgens, F. M. Mulder, M. Wagemaker, Lithium Storage in Amorphous TiO_2 Nanoparticles, J. Electrochem. Soc. 157 (2010) A582-A588

[33] J. Kim, J. Cho, Rate characteristics of anatase TiO_2 nanotubes and nanorods for lithium battery anode materials at room temperature, J. Electrochem. Soc. 154 (2007) A542-A546

[34] P.Kubiak, T. Fröschl, N. Hüsing, U. Hörmann, U. Kaiser, R. Schiller, C. K. Weiss, K. Landfester, M. Wohlfahrt-Mehrens, TiO_2 Anatase Nanoparticle Networks: Synthesis, Structure and Electrochemical Peformance, Small 7 (2011) 1690-1696

[35] J. Lin, X. Liu, S. Zhu, Y. Liu, X. Chen, Anatase TiO_2 nanotube powder film with high crystallinity for enhanced photocatalytic performance, Nanoscale Res. Lett. 10 (2015) 110

[36] R. van de Krol, A. Goossens, J. Schoonman, Spatial extent of lithium intercalation in anatase TiO_2, J. Phys. Chem. B 103 (1999) 7151-7159.

Figure captions

Fig.1. SEM micrographs of anatase TiO_2 NTAs obtained by anodic oxidation of Ti foil at a) 20V, b) 30V, c) 45V and d) 60V.

Fig. 2. XRD patterns of Ti/TiO_2 NTAs electrodes for different anodic oxidation voltages.

"●" – Anatase, "○" – Ti-foil, "∗" - Ti-metal fcc phase, "+" - TiO phase

Fig. 3. Cyclic voltammetry of Ti/TiO_2 NTAs electrodes prepared by anodic oxidation at a) 20V, b) 30V, c) 45V and d) 60V.

Fig. 4. Anodic (empty symbols) and cathodic (full symbols) peak current as function as of square root of scan rate for NTAs prepared at different anodization voltages.

Fig. 5. Areal charge/discharge capacity of NTAs electrodes, prepared at different anodic oxidation voltages, at current density 50 $\mu A \cdot cm^{-2}$.

Fig. 6. Coulombic efficiency of NTAs electrodes in 1M solution of $LiClO_4$ in propylene carbonate.

Fig 7. Voltage profiles of anatase TiO_2 NTAs for the 50^{th} cycle: a) for all anodization voltages as a function of areal capacity, b) during charge showing disappearance of nucleation barrier with amplification of anodization voltage, c) for anodic oxidation at 45 and 60 V as a function of specific capacity.

Fig. 8. Specific charge/discharge capacity of anatase TiO_2 NTAs for anodic oxidation performed at 45 and 60 V.

Table 1. Mean crystallite size of anatase phase and ratio of integral intensities of anatase and Ti-metal phase in Ti/TiO_2 NTs electrodes. These values result from the analysis of the diffraction maxima of anatase phase at ~25 degrees (2θ) and Ti-metal phase at ~40 degrees (2θ) with the XFIT software, using the Fundamental Parameter convolution approach.

Anodization voltage [V]	**Mean crystallite size [nm]**	**I_{25}/I_{40}**
20	41.3 ± 1.1	0.45
30	35.9 ± 0.7	0.70
45	32.3 ± 0.7	0.98
60	30.6 ± 0.9	0.82

Table 2. Diffusion coefficients of Li^+ ion during insertion/extraction in/from anatase TiO_2 NTs prepared by anodic oxidation at different voltages and subsequent annealing at 400°C.

Anodization voltage [V]	Calculated surface area of NTAs (per unit geometrical surface area of electrode) [cm^2]	Diffusion coefficient for Li^+ ion insertion [cm^2s^{-1}]	Diffusion coefficient for Li^+ ion extraction [cm^2s^{-1}]
20	24.2	$5.9 \cdot 10^{-15}$	$4.8 \cdot 10^{-15}$
30	37.2	$3.3 \cdot 10^{-15}$	$3.0 \cdot 10^{-15}$
45	56.8	$1.7 \cdot 10^{-15}$	$1.4 \cdot 10^{-15}$
60	77.0	$6.4 \cdot 10^{-16}$	$5.9 \cdot 10^{-16}$

Graphical Abstract (for review)

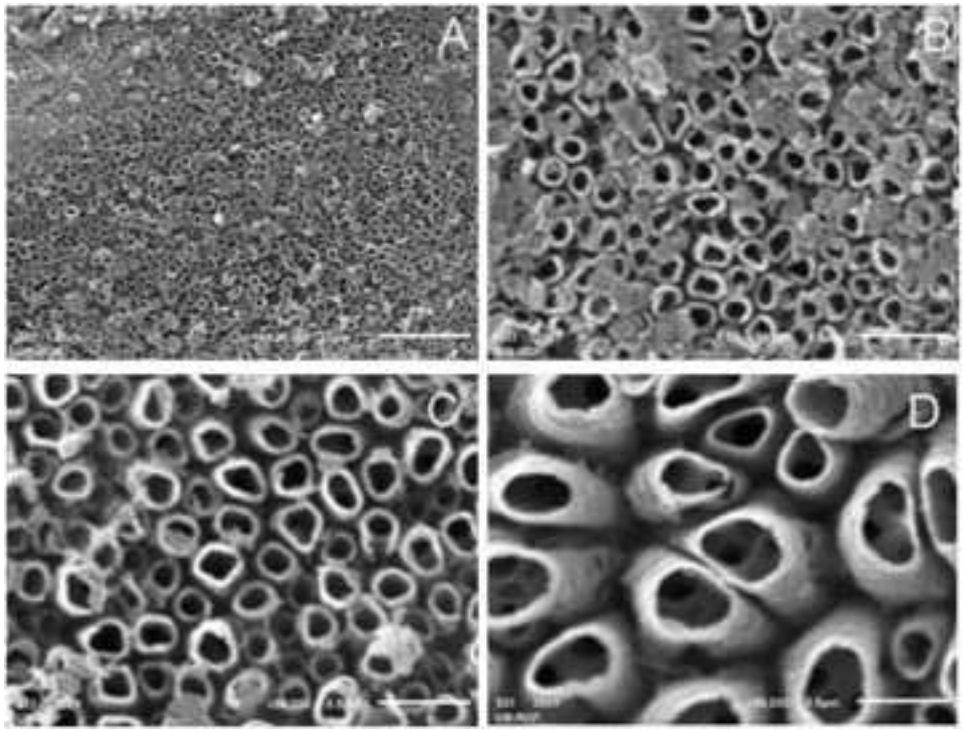

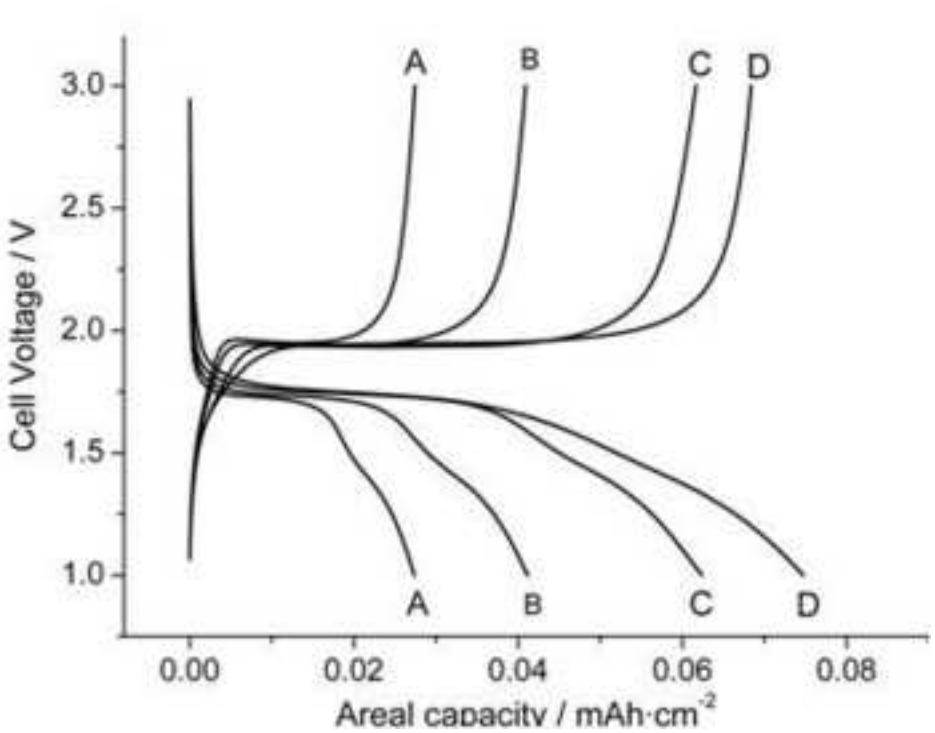

Highlights

1. Anatase TiO_2 nanotube arrays show both bulk and surface storage of Li-ion.
2. Surface area of nanotubes exposed to electrolyte depends on their morphology.
3. Absence of nucleation barrier indicates the change of lithiation mechanism.
4. Large increase in specific capacity may be attained due to the surface storage.

Table 1. Mean crystallite size of anatase phase and ratio of integral intensities of anatase and Ti-metal phase in Ti/TiO_2 NTs electrodes. These values result from the analysis of the diffraction maxima of anatase phase at ~25 degrees (2θ) and Ti-metal phase at ~40 degrees (2θ) with the XFIT software, using the Fundamental Parameter convolution approach.

Anodization voltage [V]	**Mean crystallite size [nm]**	**I_{25}/I_{40}**
20	41.3 ± 1.1	0.45
30	35.9 ± 0.7	0.70
45	32.3 ± 0.7	0.98
60	30.6 ± 0.9	0.82

Table 2

Table 2. Diffusion coefficients of Li^+ ion during insertion/extraction in/from anatase TiO_2 NTs prepared by anodic oxidation at different voltages and subsequent annealing at 400°C.

Anodization voltage [V]	Calculated surface area of NTAs (per unit geometrical surface area of electrode) [cm^2]	Diffusion coefficient for Li^+ ion insertion [cm^2s^{-1}]	Diffusion coefficient for Li^+ ion extraction [cm^2s^{-1}]
20	24.2	$5.9 \cdot 10^{-15}$	$4.8 \cdot 10^{-15}$
30	37.2	$3.3 \cdot 10^{-15}$	$3.0 \cdot 10^{-15}$
45	56.8	$1.7 \cdot 10^{-15}$	$1.4 \cdot 10^{-15}$
60	77.0	$6.4 \cdot 10^{-16}$	$5.9 \cdot 10^{-16}$

Figure 1a

Click here to download high resolution image

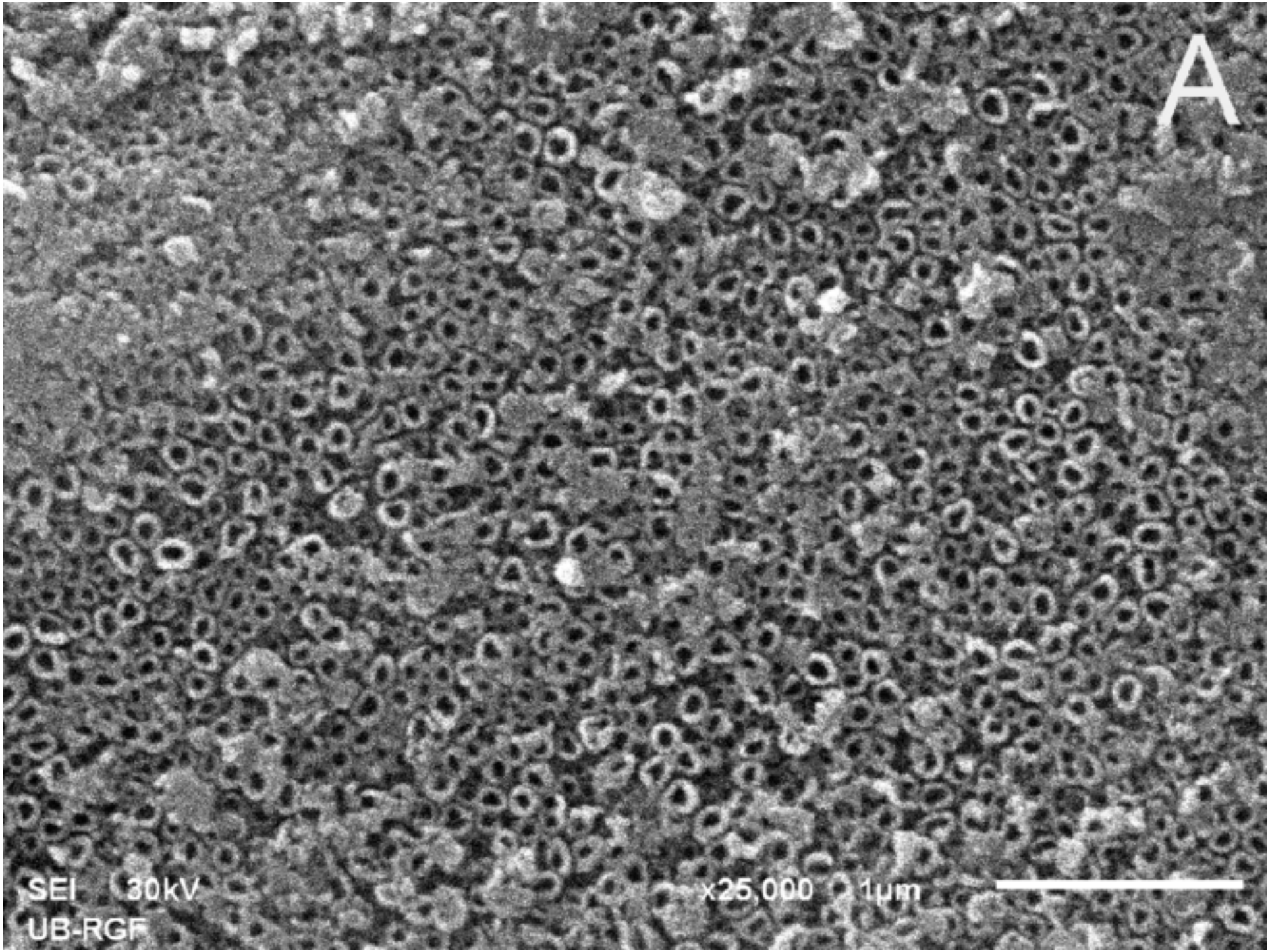

Figure 1b

Click here to download high resolution image

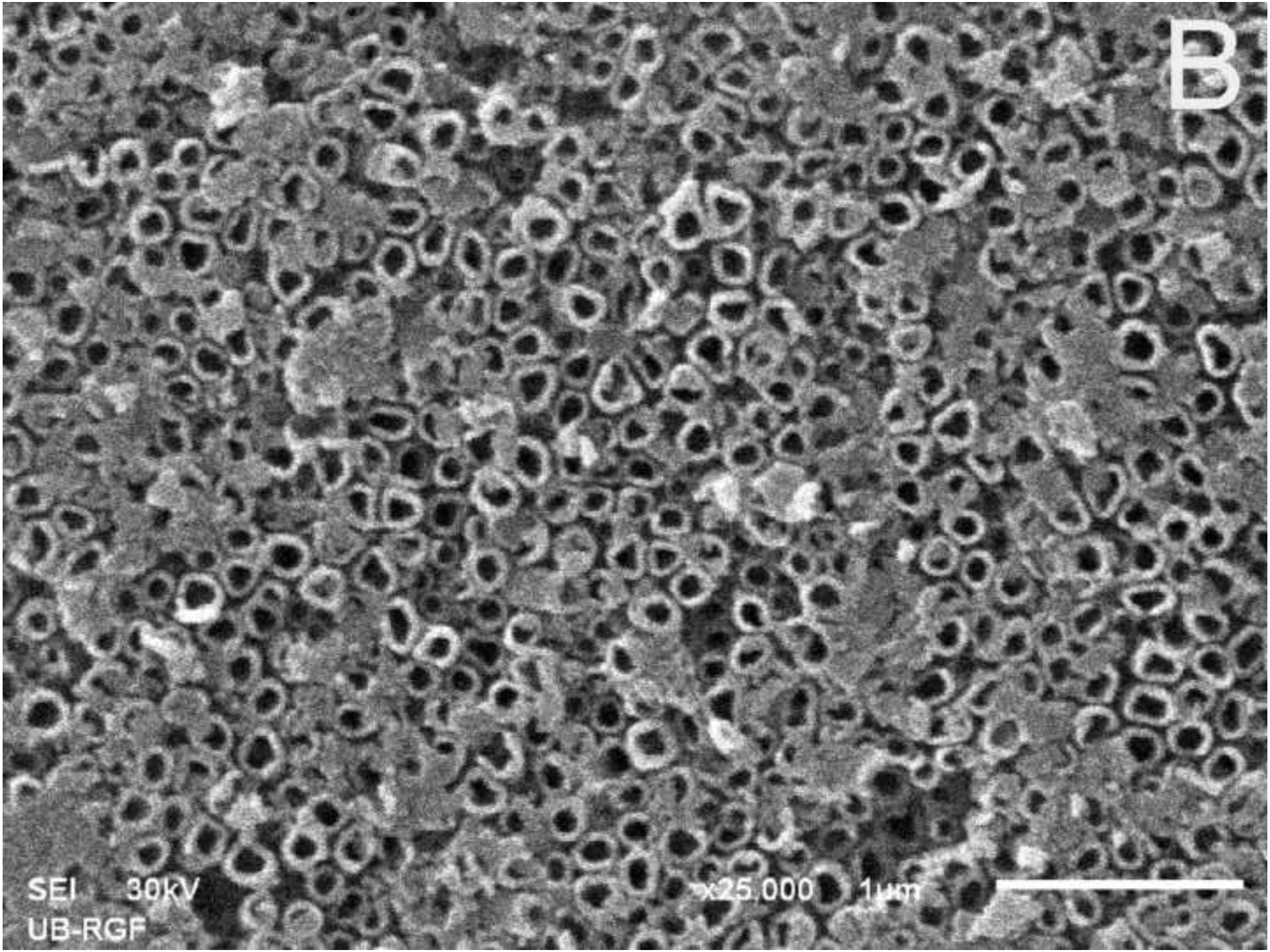

Figure 1c

Click here to download high resolution image

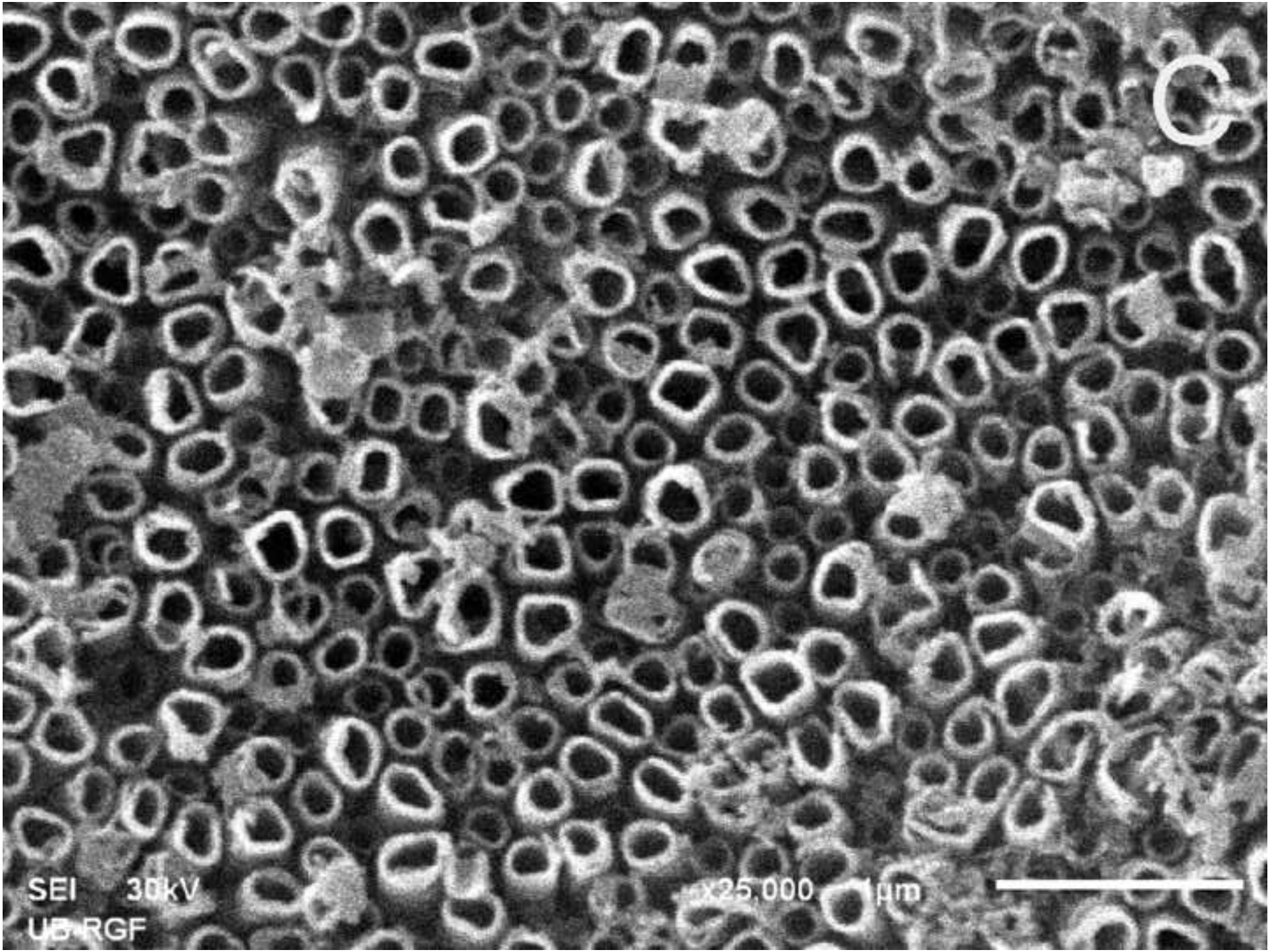

Figure 1d

Click here to download high resolution image

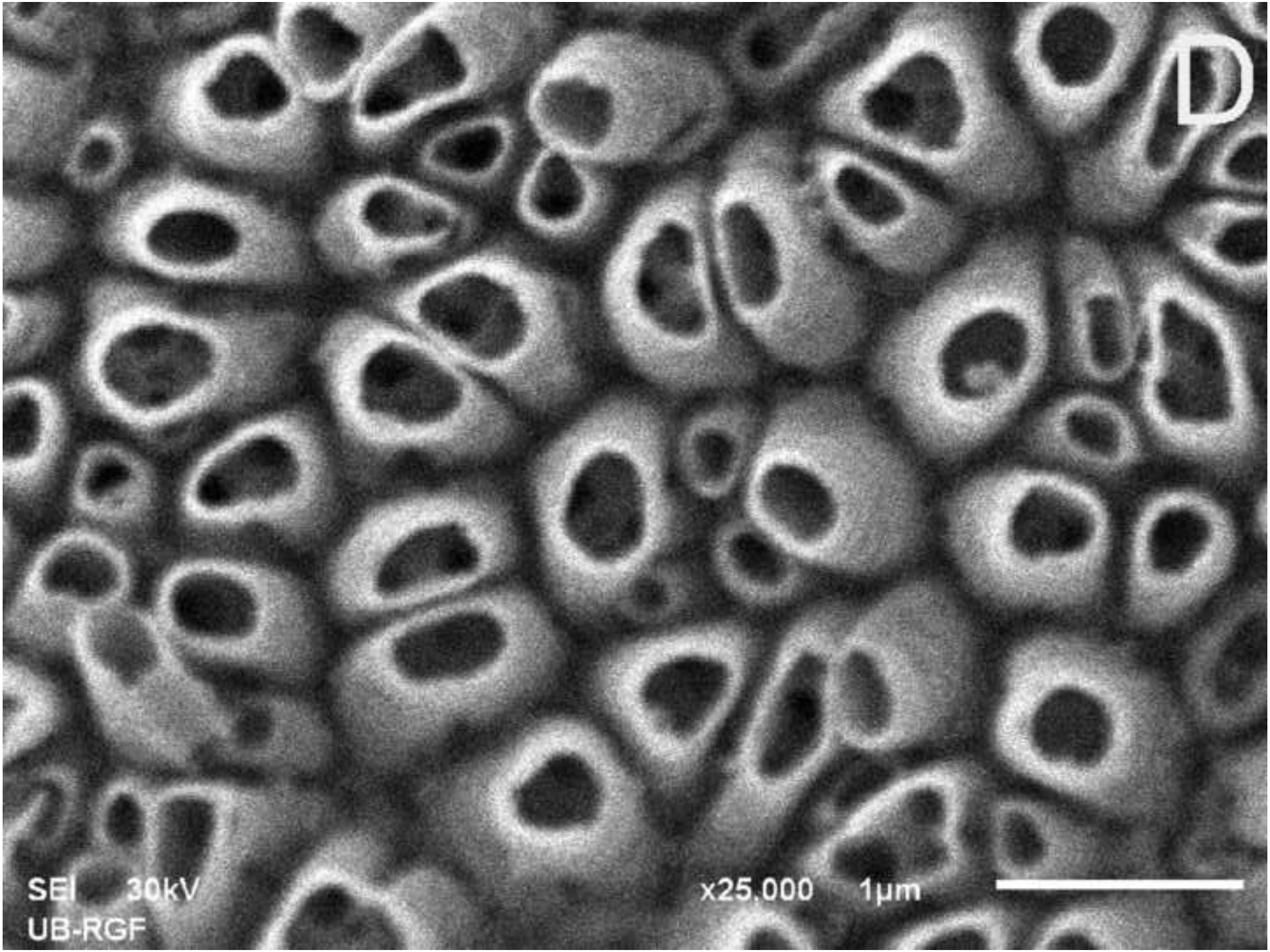

Figure 2 revised

Click here to download high resolution image

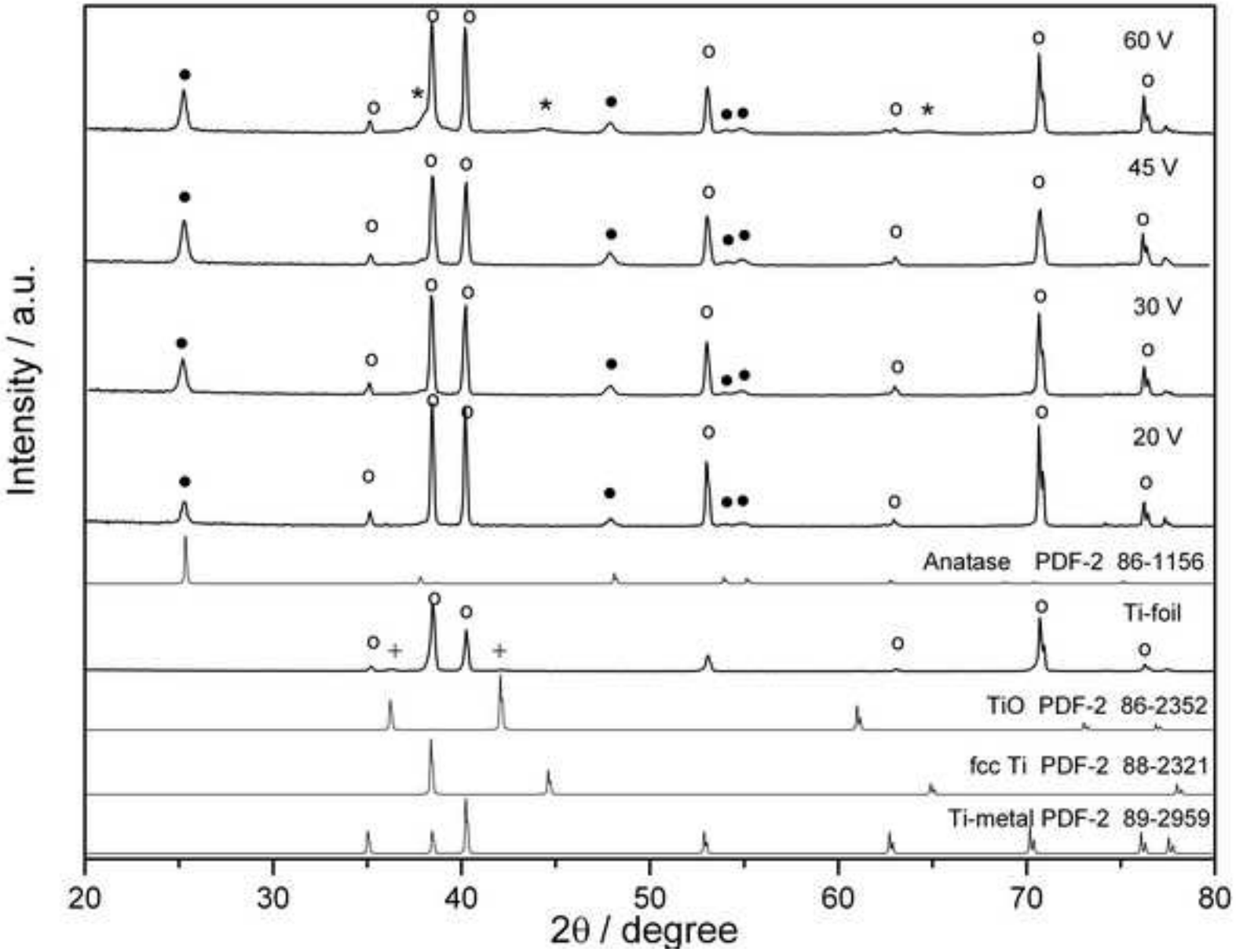

Figure 3a revised

Click here to download high resolution image

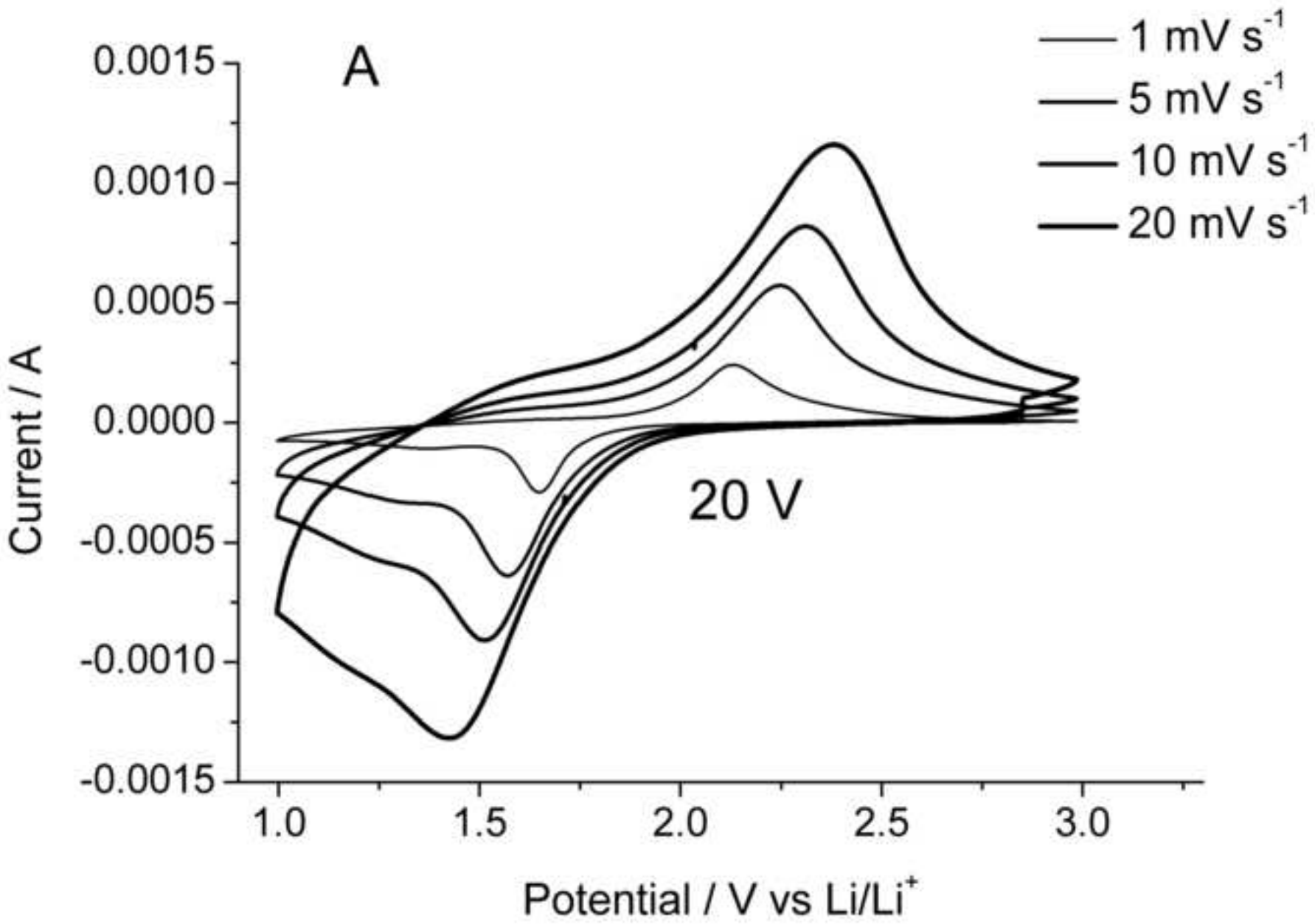

Figure 3b revised
Click here to download high resolution image

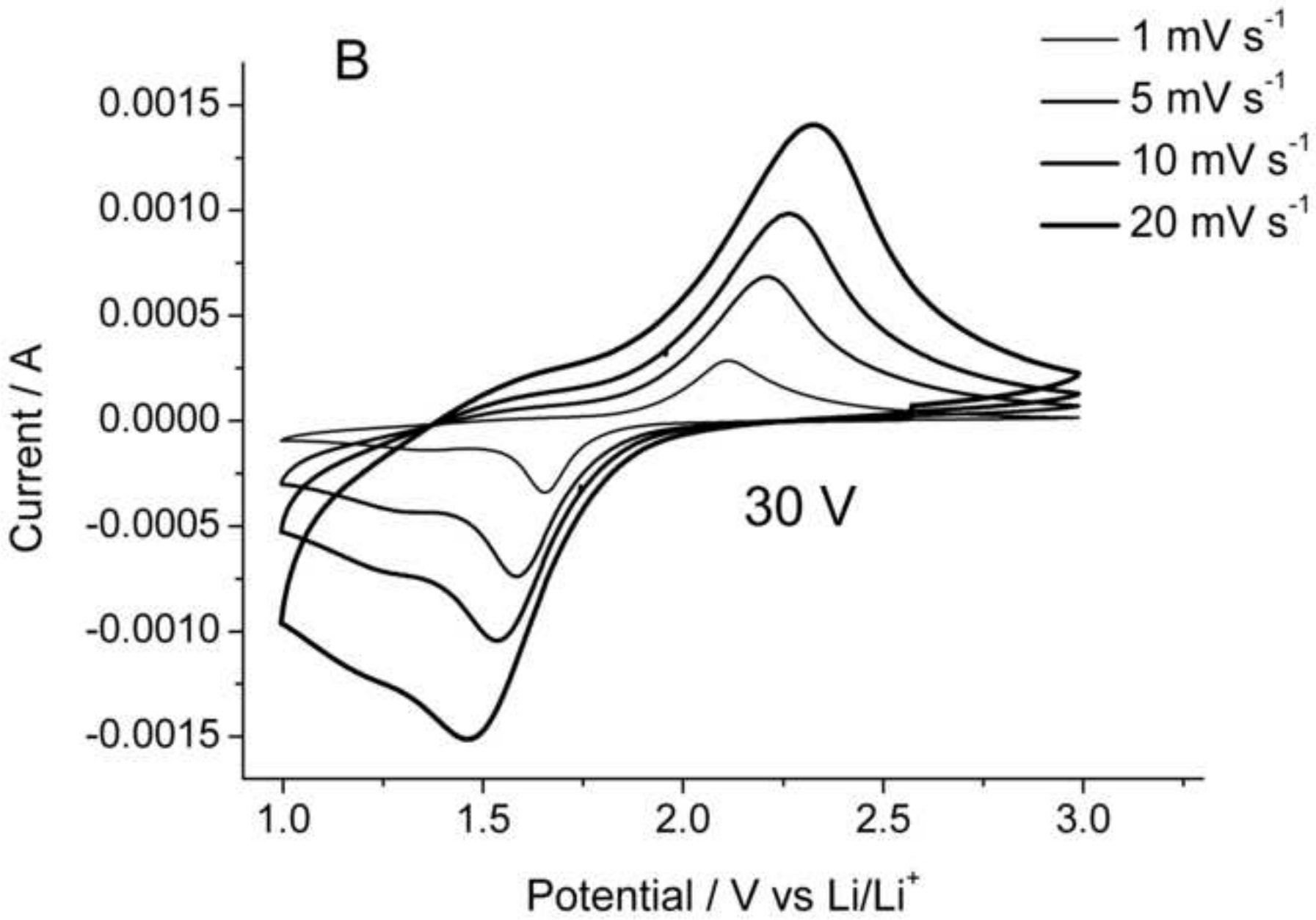

Figure 3c revised

Click here to download high resolution image

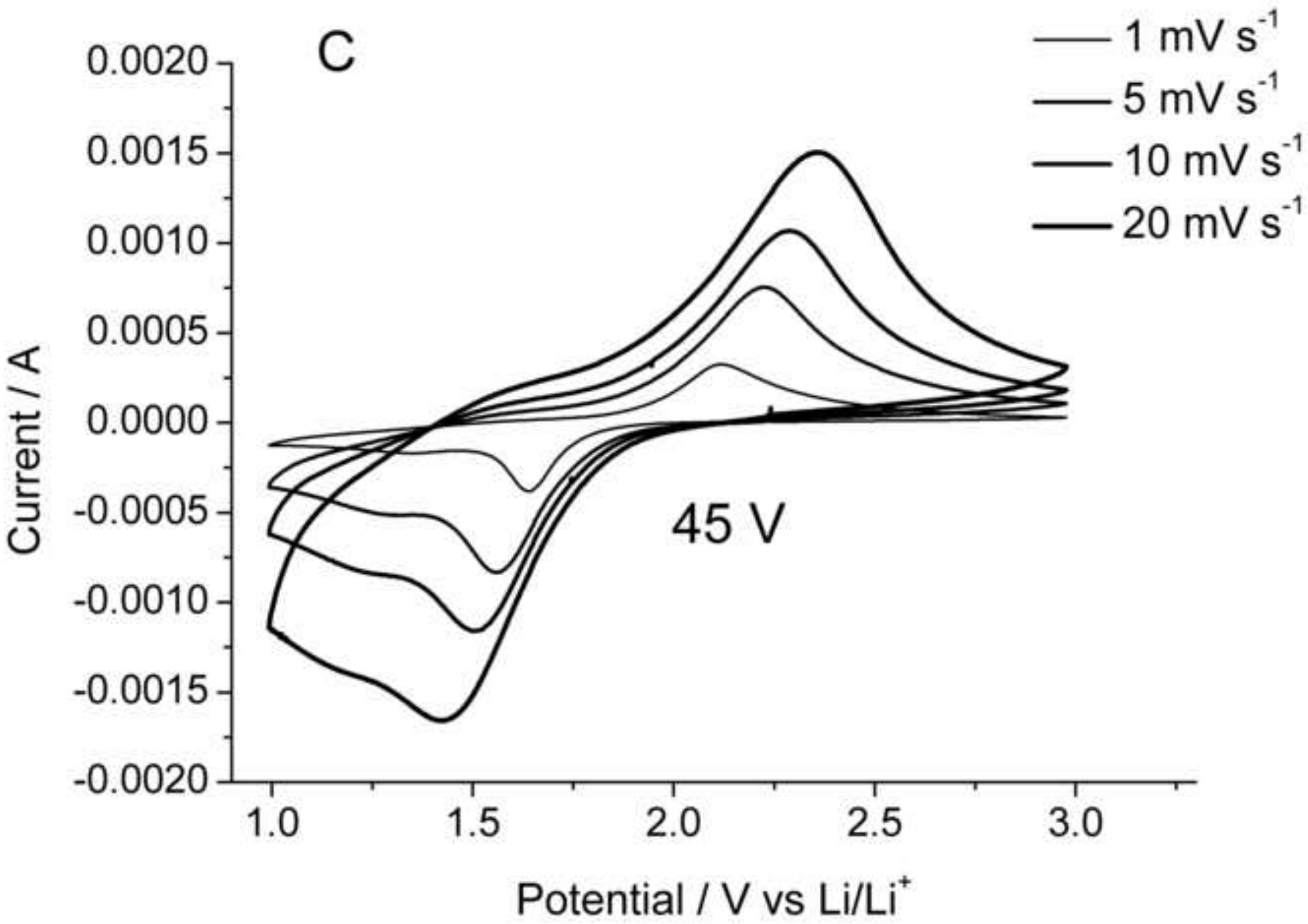

Figure 3d revised
Click here to download high resolution image

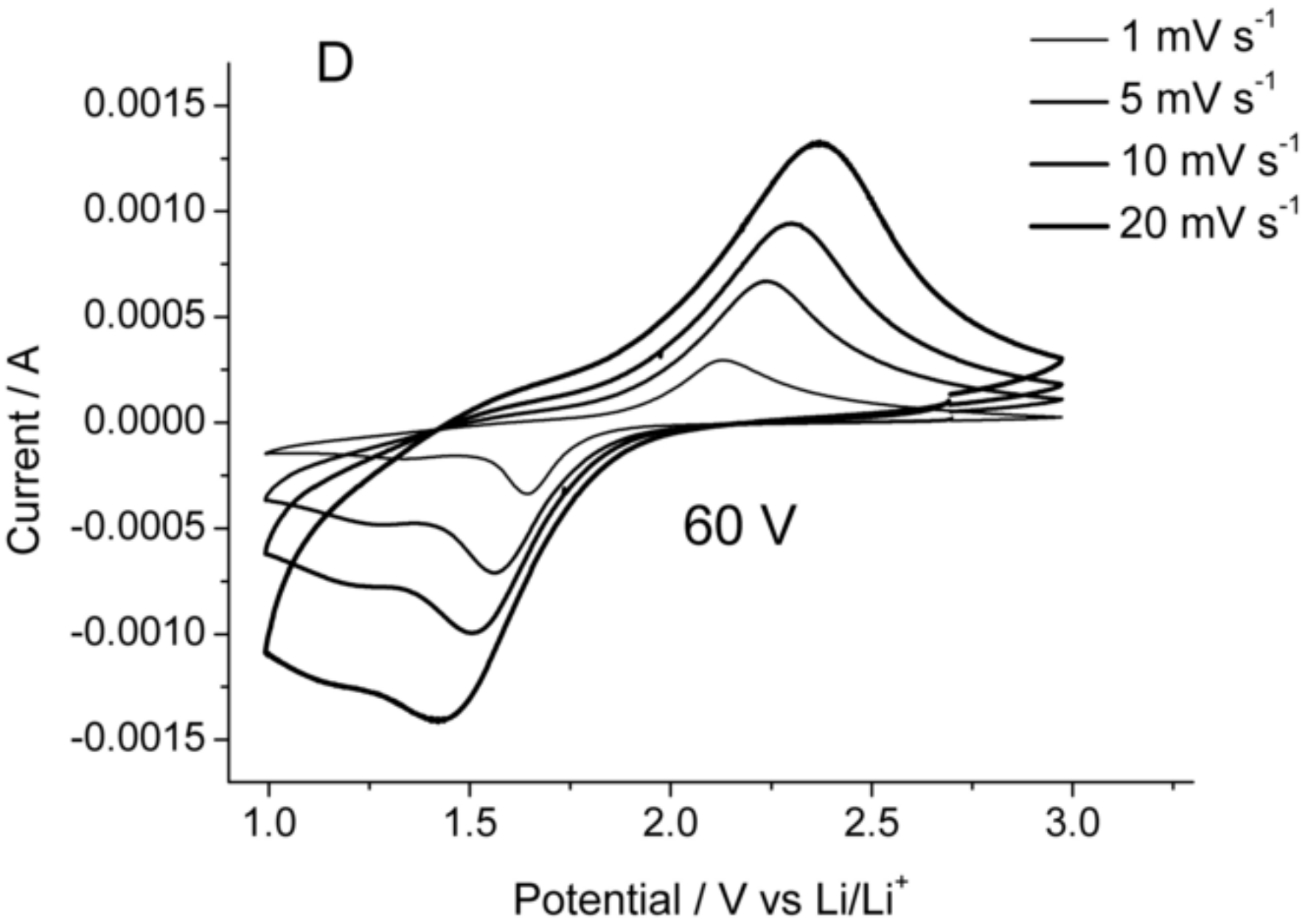

Figure 4 revised

Click here to download high resolution image

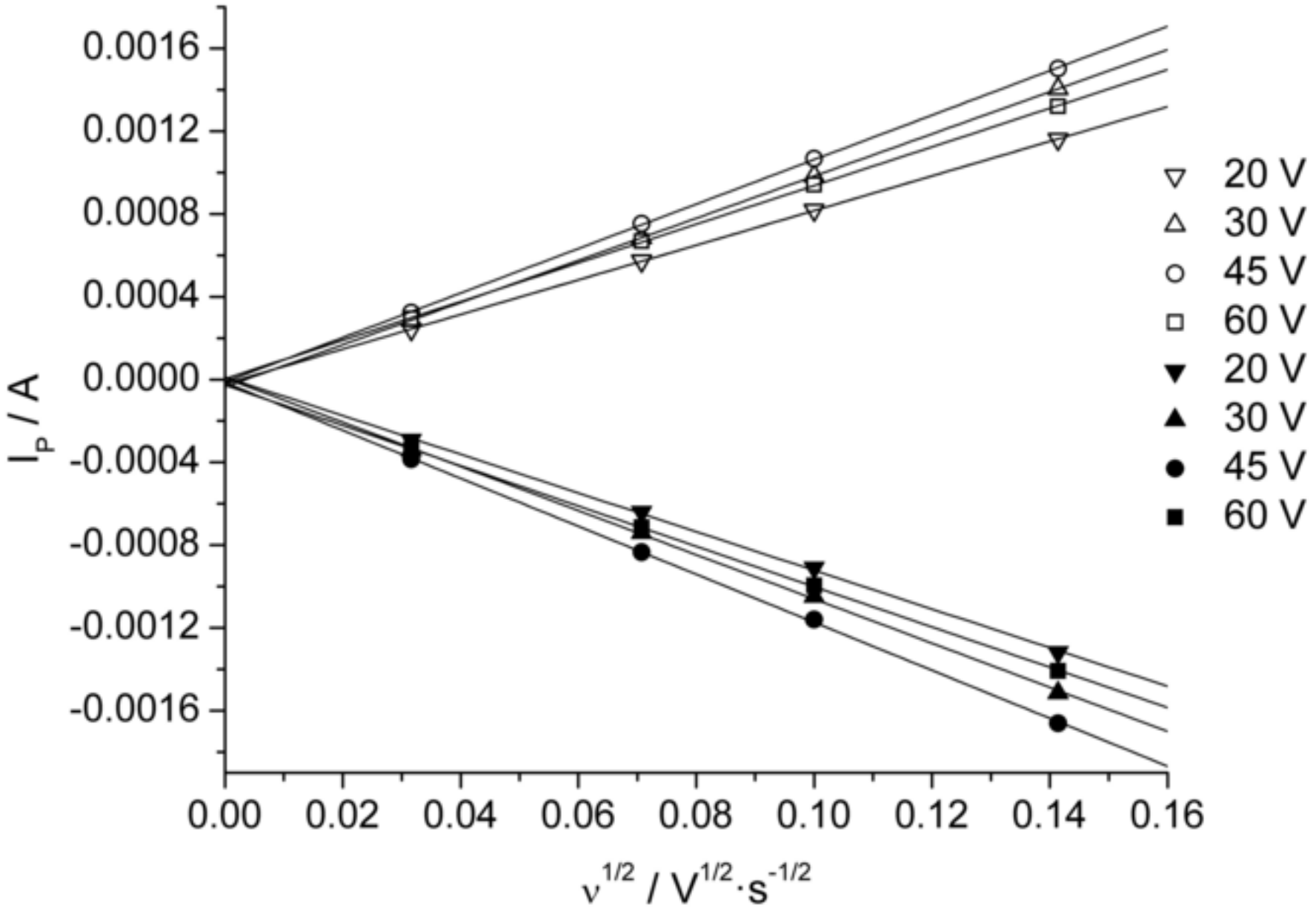

Figure 5

Click here to download high resolution image

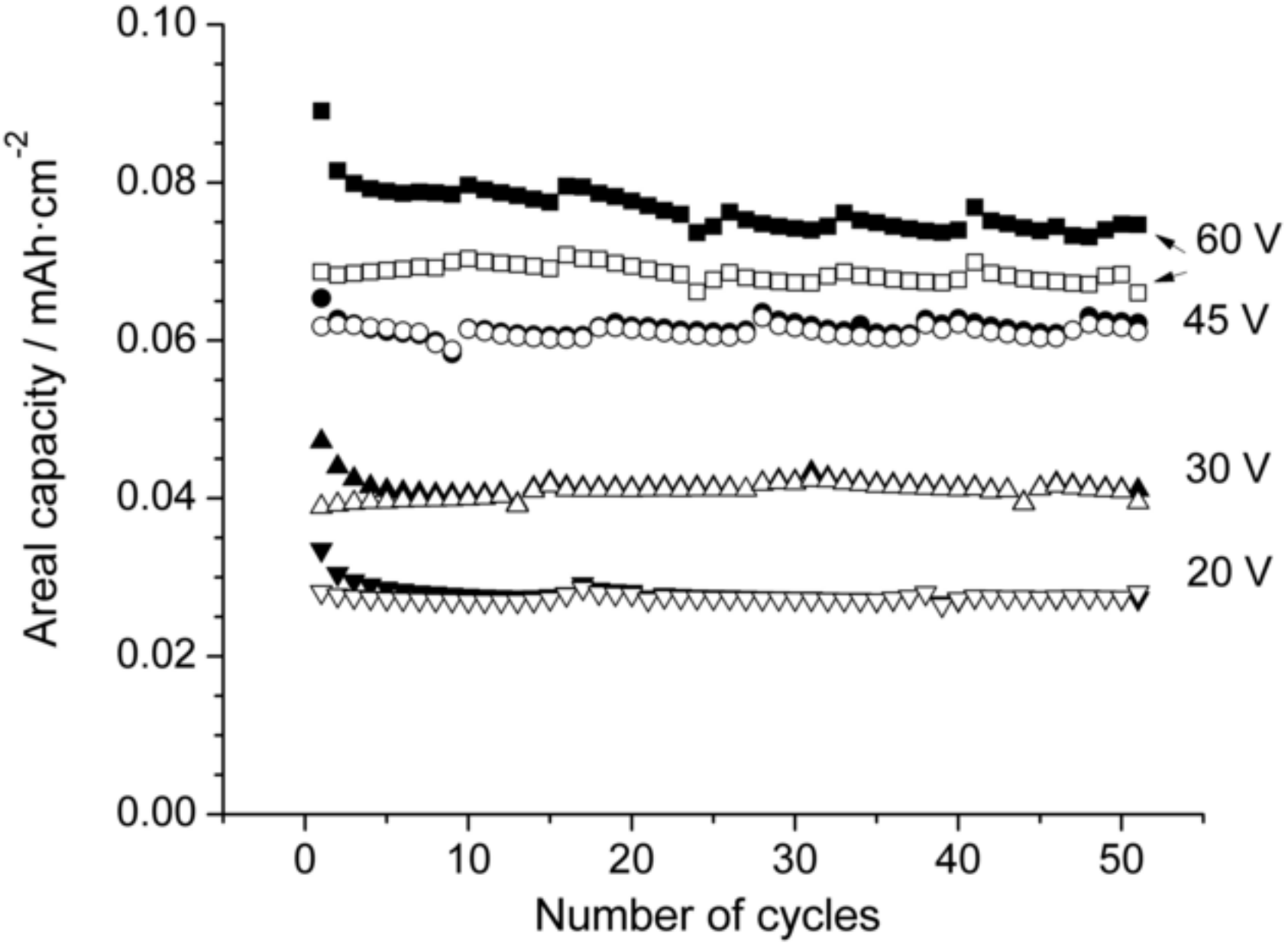

Figure 6

Click here to download high resolution image

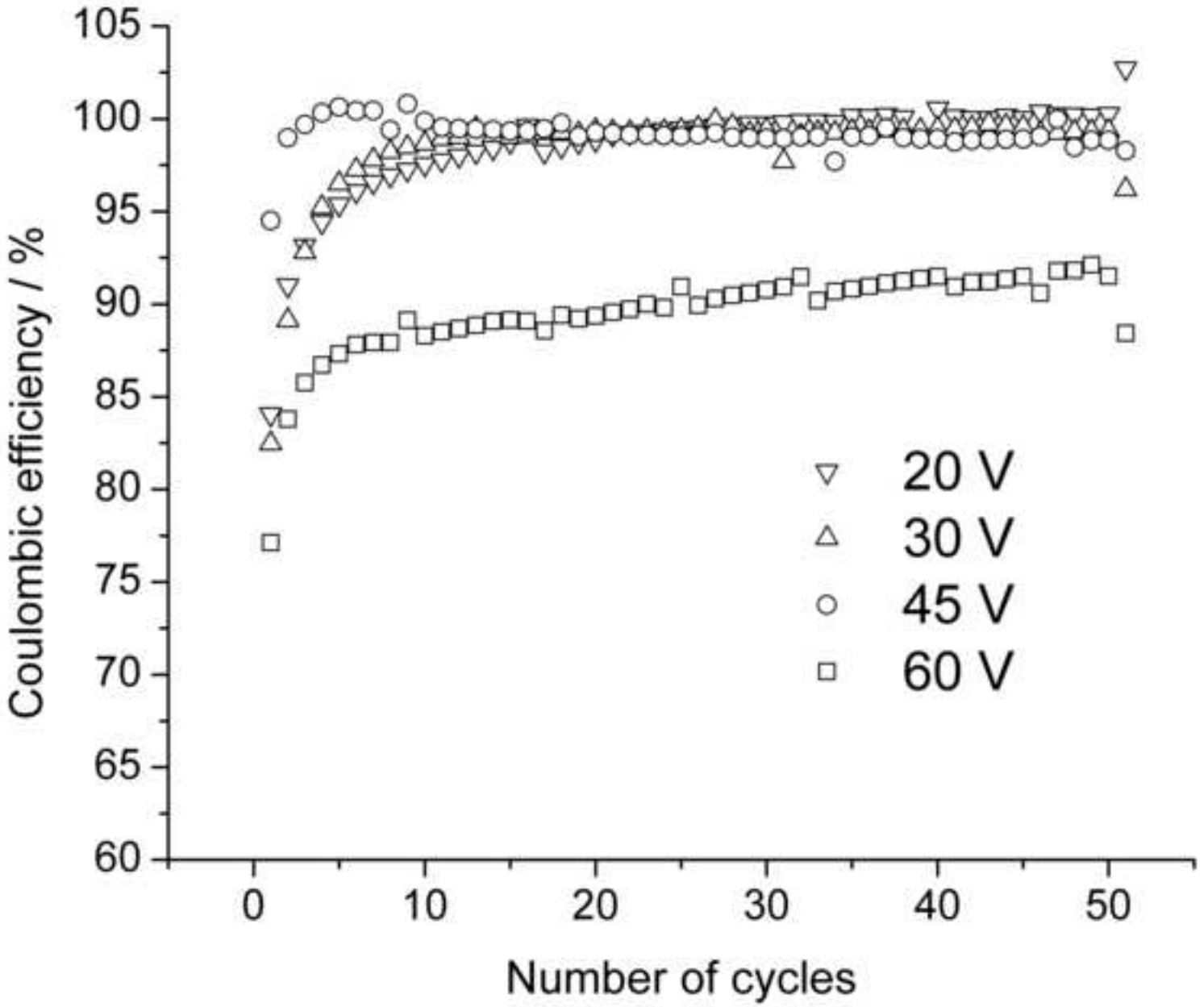

Figure 7a
Click here to download high resolution image

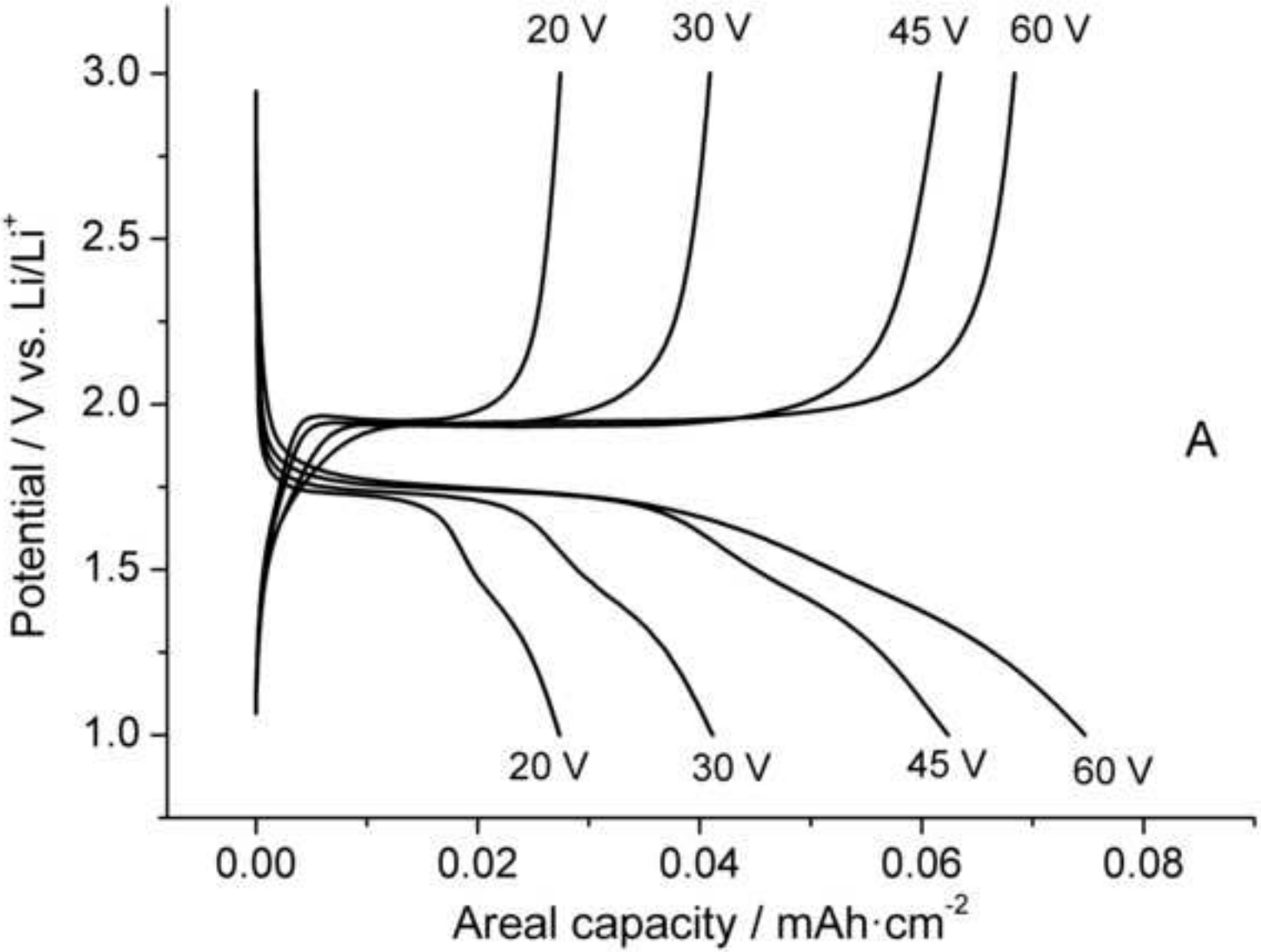

Figure 7b

Click here to download high resolution image

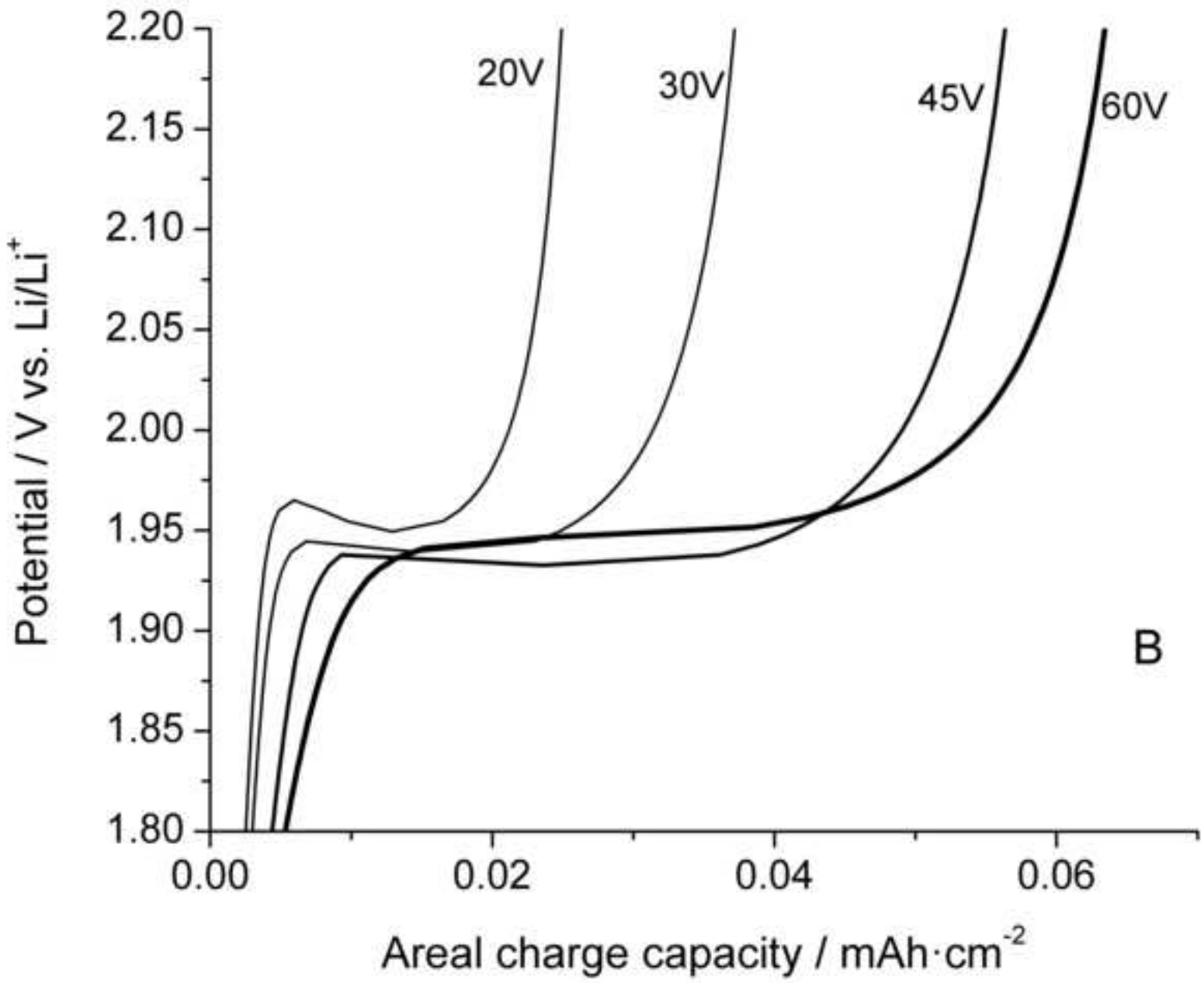

Figure 7c
Click here to download high resolution image

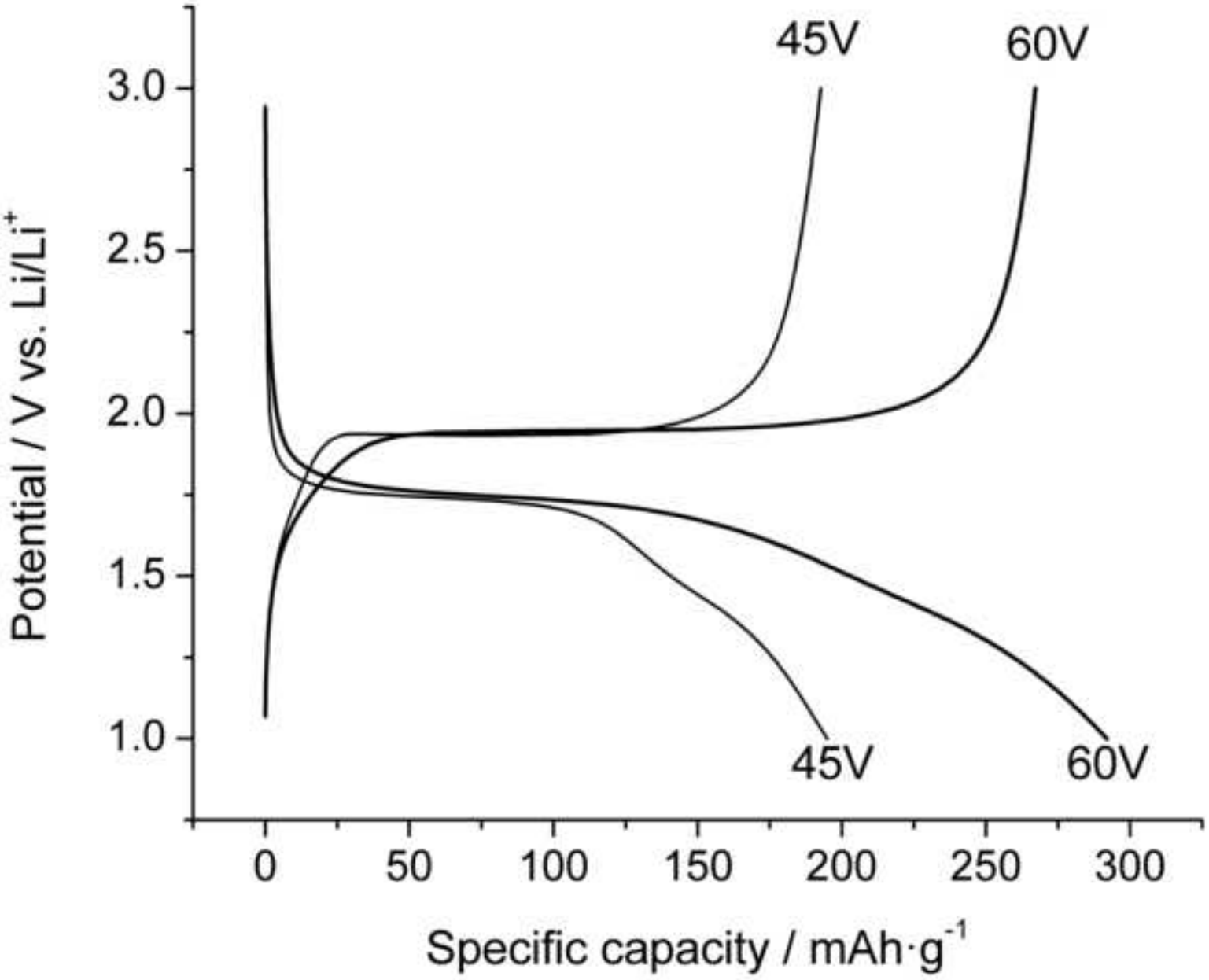

Figure 8
Click here to download high resolution image